

four quadrants, mounted at a distance of 32 mm behind the target position. Each quadrant was divided in 16 annular strips at the front side and 24 sector strips at the back side. The detection range in the laboratory frame covered angles from 16 up to 53°. Eight MINIBALL [20] clusters, consisting of three sixfold segmented HPGe crystals, were placed around the target chamber at a distance of approximately 12 cm from the target position to detect the emitted rays. An add-back procedure was applied, summing up the rays simultaneously incident on crystals of the same cluster and therefore correcting for Compton scattering within the same cluster. At an energy of 1332 keV the absolute full energy peak efficiency after applying the add-back procedure was 7.1% and at 2033 keV it was 5.6%. The total measuring time was 41 hours, the beam intensity of ^{68}Ni on the ^{108}Pd target throughout the experiment being 10^4 particles per second on average, using the production sequence as explained below. Similar Coulomb excitation experiments with this setup at comparable energies and masses have been successfully performed for the study of neutron-rich Cu and Zn isotopes [21, 22].

The only isobaric contaminant present in the beam was ^{68}Ga ($T_{1/2} = 67.63$ m), which, due to its relatively low ionization potential, was ionized at the high-temperature surface of the ion source. Moreover, the release time of ^{68}Ga from the target and ion source system (in the range of a few seconds) is much shorter than that of ^{68}Ni (in the range of a few minutes) [17]. To reduce the overwhelming contamination, considerations about the time structure of the beam are of crucial importance. The proton beam from the PS booster comes in supercycles consisting of 12 proton pulses per cycle. The individual pulses ($3 \cdot 10^{13}$ protons per pulse) are separated by a time interval of 1.2 s. Having protons on the UC_x primary target while acquiring data would cause the beam to consist mostly of the dominant ^{68}Ga contaminant, and ^{68}Ni would be a rather small component of the beam incident on the secondary ^{108}Pd target.

Due to the strong difference in release time and the pulsed proton beam structure, a specific technique can be used. For the present experiment the first few pulses of the supercycle were taken to produce the radioactive nuclei, and the ion beam gate was kept closed up to this moment (see Fig. 1). Only 800 ms after the fifth pulse the beam gate was opened, causing a considerable reduction of the rapidly releasing ^{68}Ga , whereas the ^{68}Ni isotopes were still diffusing out of the primary target ion source system with a constant rate. A similar technique has been applied in the heavy lead region [23]. To determine the beam composition, scattering data in the DSSSD detector were compared between periods when the laser beam was on (^{68}Ga and ^{68}Ni) and off (^{68}Ga only). A shutter was periodically shifted in front of the laser beam to prevent the laser light from reaching the ion source during every second supercycle. Hence, "laser on" and "laser off" data have been subsequently acquired. Figure 1 shows the number of elastically scattered par-

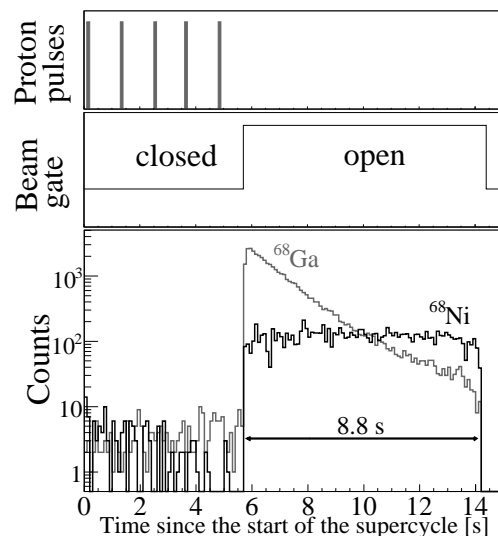


FIG. 1: Release curves for ^{68}Ni and the ^{68}Ga isobaric contaminant as a function of the time difference with the start of the supercycle. 800 ms after the fifth proton pulse the beam gate is opened, and the produced ions are sent to the experimental setup.

ticles in the DSSSD detector as a function of the time difference with the start of the 14.4 seconds long supercycle. The ^{68}Ga information has been obtained using the laser on data, whereas subtracting the laser on from the laser off data results in a pure ^{68}Ni curve. Although the ^{68}Ga contaminant is released following a quasiexponential function, ^{68}Ni is coming out almost constantly, due to the long release time of the element. The timing sequence of the proton pulses and the status of the beam gate are shown in Fig. 1 as well. This setting resulted in a ^{68}Ni to total beam intensity ratio of 24.1%. The actual measuring time when the ^{68}Ni beam was impinging on the target amounted to 8.8 seconds per supercycle (14.4-5.6 seconds). When only selecting the last 5 s of the supercycle, the ^{68}Ga contamination is lowered, enhancing the ratio of the ^{68}Ni beam component to the full beam intensity to 68.1%.

Figure 2 shows the γ -ray spectra coincident with a particle detected in the DSSSD and Doppler corrected for detection of the ^{108}Pd target recoil (a) and the ^{68}Ni scattered projectile (b), respectively, with data taken during the 8.8 s of the supercycle. The latter was zoomed around the energy of the first excited 2^+ state at 2033 keV. The Doppler-corrected spectrum for ^{108}Pd clearly shows the lines from the population of the 2_1^+ , 2_2^+ , and 4_1^+ states in the target. Two smeared out photo peaks from the transitions in the ^{68}Ga contaminant are also visible. The events shown in both spectra are in prompt coincidence with the detection of a particle in the silicon strip detector, which can be the projectile or the target or both. The energy deposited in the DSSSD detector as a function of the laboratory angle allows the projectile (^{68}Ni)

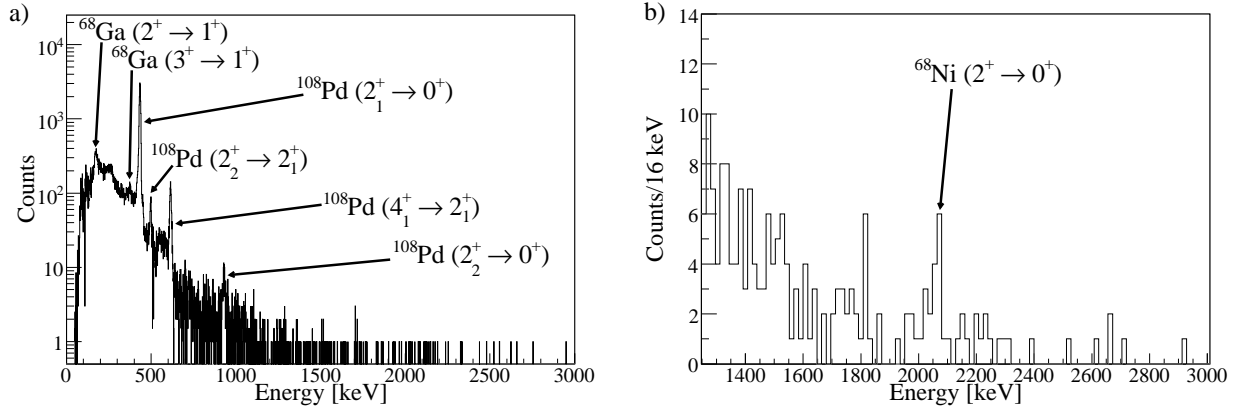


FIG. 2: γ -ray spectrum with particle coincidence Doppler corrected for ^{108}Pd target excitation (a) and part of the γ -ray spectrum with particle coincidence Doppler corrected for ^{68}Ni projectile excitation (b) focused around 2033 keV.

and ^{68}Ga) and target (^{108}Pd) ions to be discriminated. The following procedure was used to perform the Doppler correction (see Fig. 3). In case a Doppler-shifted 2033-keV γ -ray is emitted by the ^{68}Ni projectile, knowledge on the direction and the energy of the scattered ion is required to perform the Doppler correction. If the ^{68}Ni nucleus is detected in the DSSSD detector, these quantities are registered in a direct way. This occurs when the projectile has been scattered between 16 and 53 in the laboratory system (26 and 83 in the center-of-mass frame). In case a ^{108}Pd target particle was detected in the silicon strip detector, the ^{68}Ni projectile was scattered between 46 and 112 in the laboratory system (73 and 148 in the center-of-mass frame). Only in the small range between 46 and 53 (73 and 83 in the center-of-mass frame) the projectile was detected as well, and this happens of course in opposite quadrants. If the angle of the projectile is higher, the registered position and energy of the associated target recoil of the collision were used to infer the direction and the energy of the scattered ^{68}Ni projectile, assuming inelastic scattering in two-body kinematics, hereby correcting for the energy loss in the target. Applying this method enlarges substantially the center-of-mass angular range used to integrate the cross section, increasing the statistics in the particle-coincident γ -ray spectrum with a factor of 2.7 for ^{68}Ni and 2.6 for ^{108}Pd . Figure 3 shows how the scattering angles of projectile and target are correlated in the laboratory frame as a function of the angle in the center-of-mass frame, indicating the angular range covered by the DSSSD detector. Parts of the angular range outside the detection range of the DSSSD are now included by indirectly deriving direction and energy of the nondetected nucleus emitting the γ -ray. All events registered occur at a center-of-mass angle lower than 150° , insuring the safe nature of the Coulomb excitation process. When exceeding this angle, nuclear effects can no longer be excluded, as the distance between the surfaces of the two colliding nuclei becomes smaller than 5 fm .

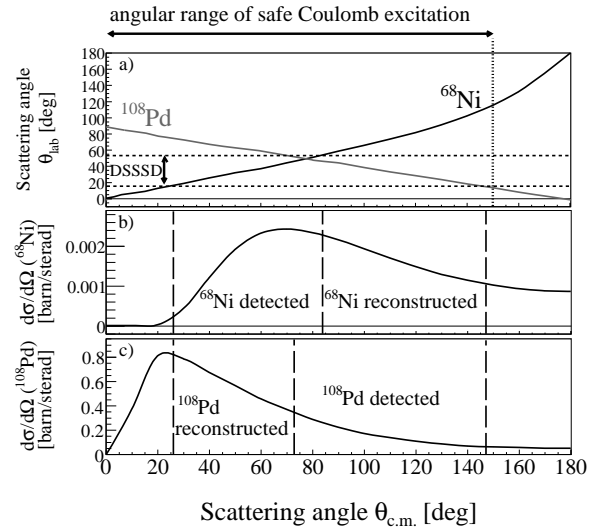


FIG. 3: Scattering angles of the ^{68}Ni projectile and the ^{108}Pd target particles in the laboratory frame versus the scattering angle in the center-of-mass frame (a). From the angular range of the DSSSD detector it can be seen where the information on the emitting nucleus was registered directly and where it was deduced indirectly. Also the differential cross sections for both nuclei are shown (b and c). All detected events occur in the angular range of safe Coulomb excitation, where the distance between the nuclear surfaces never exceeds 5 fm .

In Fig. 2(b) a peak structure of 11 counts is visible around 2 MeV on a constant background of 1 count per 16 keV energy bin. The photo peak energy 2050 \pm 65 keV corresponds well to the known value of 2033 keV. This peak is therefore assigned to the $2^+ \rightarrow 0^+$ transition in ^{68}Ni resulting in a total number of counts 11^{+5}_4 . The asymmetry in the error bar is due to the low number of counts, implying the use of Poisson statistics [24]. As the figure shows only the high-energy events, the strongest Coulomb excitation lines of ^{68}Ga , which are for this odd-

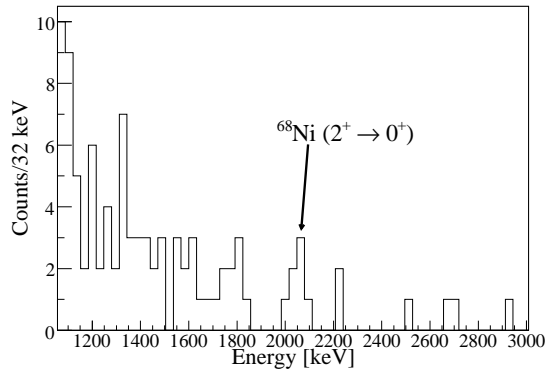


FIG. 4: Particle-coincident γ -ray spectrum Doppler corrected for ^{68}Ni . Only the events occurring within the last 5 s of the proton pulse supercycle are included.

odd nucleus mainly of low-energy nature, are not visible. A separate article will discuss the Coulomb excitation information on the Ga contaminant.

A consistency check was performed by selecting the γ -ray events occurring within the last 5 s of the supercycle, resulting in a suppression of the ^{68}Ga lines, and therefore decreasing the background. Figure 4 shows the γ -ray events with the same conditions as the ^{68}Ni spectrum in Fig. 2, but with this time selection in the supercycle. Integrating the photo peak at 2033 keV in this ^{68}Ni -enhanced spectrum results in 7 prompt counts and 1 count in the background, yielding a rate of 6^{+3}_2 counts. The time selection (of the last 5 s) covers 57% of the total time of the supercycle when the beam was incident on the ^{108}Pd target (8.8 s). Due to the fact that ^{68}Ni is released constantly, the amount of excitations in the nucleus should decrease by approximately 57% when using the time selection. The counting rate of 6^{+3}_2 in the ^{68}Ni -enhanced spectrum is therefore consistent with the 11^{+5}_4 de-excitations seen in the γ -ray spectrum without a time selection in the supercycle. The amount of ^{68}Ga

within this supercycle time selection is 8% compared to the full statistics, as can be calculated from the elastically scattered particles in the DSSSD detector during laser on/off data (Fig. 1). Comparing the γ -ray intensity of $2^+ \rightarrow 1^+$ transition in ^{68}Ga results in a value of 7%, again confirming the consistency of this method.

Of the 11^{+5}_4 counts in the de-excitation photo peak, the cross section for exciting ^{68}Ni to its first 2^+ state was determined using the program GOSIA 2 [25], which calculates the γ -ray yields after integration over the scattering ranges and energy loss in the target, taking into account the angular distribution of the γ -rays. Hereby the quadrupole moment of the 2^+ state was assumed to be small and the reorientation effect was neglected. The amount of de-excitations in the photo peak of the known $2^+ \rightarrow 0^+$ transition in ^{108}Pd [26] was used for normalization, correcting it for ^{68}Ga -induced excitation. The uncertainty on the count rate in the target de-excitation photo peak contributed only 3% to the total error. The experimentally measured $B(E2)$ value in ^{68}Ni was $2.8^{+1.2}_{-1.0} \cdot 10^2 \text{ e}^2 \text{ fm}^4$. This result is less accurate but in good agreement with the value measured using Coulomb excitation at intermediate energy (255 MeV), confirming the low transition probability of 260 MeV from a weighted average.

Studies involving safe Coulomb excitation experiments on more neutron-rich nickel isotopes are not hindered by the in-target production using proton-induced fission but by the slow release out of the target matrix and the strong contamination of the gallium isobars. Vigorous research is needed to bring down this delay time to the required seconds range and to reduce the gallium contamination to extend this study toward the doubly magic ^{78}Ni nucleus. Work in this direction is underway at ISOLDE [16].

This work was supported by EU Sixth Framework through No. EURONS-506065, BM BF under Contract No. 06KY 205I and No. 06MT 238, BRX JAP Research Program No. P6/23, and FWO-Vlaanderen (Belgium). We acknowledge fruitful discussions with K. Rissager.

-
- [1] W. M. Ueller et al., Phys. Rev. Lett. 83, 3613 (1999).
 [2] R. Broda et al., Phys. Rev. Lett. 74, 868 (1995).
 [3] O. Sorlin et al., Phys. Rev. Lett. 88, 092501 (2002).
 [4] C. Guenaut et al., Phys. Rev. C 75, 044303 (2007).
 [5] S. Raha et al., Eur. Phys. J. A 34, 5 (2007).
 [6] M. Bemas et al., Phys. Lett. B 113, 279 (1982).
 [7] T. Ishii et al., Phys. Rev. Lett. 84, 39 (2000).
 [8] J. Van Roosbroeck et al., Phys. Rev. C 69, 034313 (2004).
 [9] O. Peru et al., Phys. Rev. Lett. 96, 232501 (2006).
 [10] K. Kaneko et al., Phys. Rev. C 74, 024321 (2006).
 [11] H. Grawe and M. Lewitowicz, Nucl. Phys. A 693, 116 (2001).
 [12] K. Langanke et al., Phys. Rev. C 67, 044314 (2003).
 [13] D. Cline, Ann. Rev. Nucl. Part. Sci. 36, 683 (1986).
 [14] V. Mishin et al., Nucl. Instr. and Meth. B 73, 550 (1993).
 [15] U. Koster et al., Spectrochim. Acta B. 58, 1047 (2003).
 [16] V. Fedoseyev et al., Hyp. Inter. 127, 109 (2000).
 [17] U. Koster, Ph.D. thesis, T. U. München (2000).
 [18] D. Habs et al., Nucl. Instr. and Meth. B 139, 128 (1998).
 [19] A. N. Ostrowski et al., Nucl. Instr. and Meth. A 480, 448 (2002).
 [20] J. Eberth et al., Prog. Part. Nucl. Phys. 46, 389 (2001).
 [21] I. Stefanescu et al., Phys. Rev. Lett. 98, 122701 (2007).
 [22] J. Van de Walle et al., Phys. Rev. Lett. 99, 142501 (2007).
 [23] P. Van Duppen et al., Nucl. Instr. and Meth. B 134, 267 (1998).
 [24] W. A. Rolke et al., Nucl. Instr. and Meth. A 458, 745 (2001).
 [25] T. Czosnyka, computer code GOSIA 2, University of Warsaw (2005).
 [26] L. Svensson et al., Nucl. Phys. A 584, 547 (1995).